

Revised Manuscript:
J. Biol. Chem.

Identification of a zinc finger domain in the human NEIL (Nei like)-2 protein

Aditi Das¹, Lavanya Rajagopalan¹, Venkatarajan S. Mathura²,
Samuel J. Rigby³, Sankar Mitra¹ and Tapas K. Hazra^{1*}

¹Sealy Center for Molecular Science and Department of Human Biological
Chemistry and Genetics, University of Texas Medical Branch, Galveston,
Texas, USA 77555-1079, ²Roskamp Institute, Sarasota, FL, ³Department
of Geology, Scripps Institution of Oceanography, La Jolla, CA

Running Title: Zinc finger motif in NEIL2

*Corresponding author: Sealy Center for Molecular Science, University of Texas Medical
Branch, 6.136 Medical Research Building, Route 1079, Galveston, Texas, USA. Telephone: 409-
772-2156, Fax: 409-747-8607. E-mail: tkhazra@utmb.edu

Summary

The recently identified human NEIL (Nei like)-2 protein, a DNA glycosylase/AP lyase specific for oxidatively damaged bases, shares structural features and reaction mechanism with the *Escherichia coli* DNA glycosylases, Nei and Fpg. Amino acid sequence analysis of NEIL2 suggested it to have a Zn-finger like Nei/Fpg. However, the Cys-X2-His-X16-Cys-X2-Cys (CHCC) motif present near the C-terminus of NEIL2 is distinct from the Zn-finger motifs of Nei/Fpg, which are of the C4 type. Here we show the presence of an equimolar amount of Zn in NEIL2 by inductively coupled plasma mass spectrometry. Individual mutations of C291, H295, C315 and C318, candidate residues for coordinating Zn, inactivated the enzyme by abolishing its DNA-binding activity. H295A and C318S mutants were also shown to lack bound Zn and a significant change in their secondary structure was revealed by CD spectra analysis. Molecular modeling revealed R310 of NEIL2 to be a critical residue in its zinc-binding pocket, which is highly conserved throughout the Fpg/Nei family; an R310Q mutation significantly reduced NEIL2's activity. We thereby conclude that the Zn-finger motif in NEIL2 is essential for its structural integrity and enzyme activity.

Introduction

Oxidative DNA damage has been implicated in mutagenesis, and is suggested to be involved in the etiology of aging and many diseases, including cancer (1,2). Repair of oxidatively damaged bases in all organisms occurs primarily via the DNA base excision repair pathway (BER), which is initiated with excision of damaged bases by DNA glycosylases (3). Until recently, only two DNA glycosylases, NTH1 (endonuclease III homolog) and OGG1 (8-oxoguanine DNA glycosylase), have been characterized in mammals, which are responsible for repair of oxidized pyrimidine and purine base lesions respectively. Both OGG1 and NTH1,

orthologs of the *E. coli* glycosylase, Nth, utilize an internal Lys residue as the active site nucleophile, and carry out β -elimination at the abasic (AP) site generated after base removal (4,5). However, *E. coli* has two other oxidized base-specific DNA glycosylases, namely MutM/Fpg and its paralog Nei (6,7) which utilize the N-terminal Pro as the active site nucleophile (8) and carry out $\beta\delta$ elimination at the AP site after excising the base lesion. We and others recently discovered and characterized two other mammalian DNA glycosylases and named these NEIL (Nei like)-1 and -2, which are orthologs of *E. coli* Fpg/Nei (9-13). Both NEILs use the N-terminal Pro as the active site, and function as a DNA glycosylase/ AP lyase to carry out $\beta\delta$ -elimination (9,10). The recombinant NEILs are active in excising a variety of oxidatively damaged bases, but show significant differences in substrate preference. NEIL1 prefers ROS-derived pyrimidines lesions, and also efficiently removes FapyG and FapyA, ring-opened oxidation products of purines (9,12). NEIL2 removes oxidized pyrimidine substrates from duplex DNA, but is more efficient in excising oxidized bases when they are located in a DNA bubble structure (14).

NEIL2 shares overall identity of 32 and 27 % with Fpg and Nei, respectively, and the key residues of the *E. coli* enzymes, in particular the N-terminal PE(L/G)P(E/L) motif, are completely conserved in NEIL2 (10). In contrast to the Nth family, the Fpg/Nei family utilizes two DNA-binding motifs, a helix-two turn-helix (H2TH) (15) and a Zn-finger motif (16). Fpg and Nei share significant homology with each other, including the sequence of the zinc finger motif which is of the C4 type (17). The Zinc finger motifs are often involved in specific DNA recognition, and have been identified in many DNA-binding proteins, transcription factors and products of developmental control genes (18-21). Furthermore, several proteins associated with DNA repair, like Xeroderma Pigmentosum complementation group A (XPA), poly ADP-ribose

polymerase (PARP) and replication-associated protein A (RPA) have been shown to contain Zn-finger domains (22-25). In *E. coli*, the UvrA protein, which is involved in DNA damage recognition during nucleotide excision repair, also possesses Zn-finger domain (26,27). Identification of Zn-finger motifs in the ever-growing number of DNA-binding proteins is based primarily on the presence of conserved Cys or His residues and the spacing between them, which may be critical in recognition of specific double stranded DNA sequences.

Here we show that NEIL2 possesses a single unusual CHCC-type Zn-finger motif at its C-terminus, which is distinct from that of Nei/Fpg, and that this motif is essential for maintaining the structural integrity and activity of NEIL2.

Experimental Procedures

Expression of wild-type and mutant NEIL2 polypeptides

The wild-type (WT) full-length NEIL2 was cloned between the *NdeI/XhoI* sites of the expression plasmid pRSETB (Invitrogen) (10). The NEIL2 mutants (C291S, H295A, C315S, C318S as well as R310A) were generated using a site-directed mutagenesis kit (Stratagene), and their authenticity was confirmed by direct DNA sequencing.

Log-phase cultures of *E. coli* DE884 *mutM nei* were transformed with expression plasmids of WT and mutant NEIL2 and then induced with 0.2 mM IPTG at 16°C for 16 h. After centrifugation, the cell pellets were suspended in a lysis buffer-containing 20 mM Tris-HCl, pH 7.5, 150 mM NaCl, 1 mM EDTA, 100 µg/ml lysozyme, 5 mM dithiothreitol (DTT) and protease inhibitor cocktail. After sonication and centrifugation, the supernatant was used for Western blot analysis or activity assay by trapping analysis (10).

Purification of anti-NEIL2 antibody and Western blot analysis

Polyclonal anti-NEIL2 antibodies were purified from rabbit antisera produced by Alpha Diagnostics (San Antonio, Texas) by affinity chromatography on Sepharose 4B (Amersham Pharmacia) covalently coupled to NEIL2. NEIL2-specific IgG was eluted with Glycine-HCl (pH 2.8) and immediately neutralized with 0.1 volume of 1M Tris base, and stored at -80°C after concentration (Amicon) and dialysis in phosphate-buffered saline (PBS).

Lysates of *E. coli* (2 μg) expressing WT and mutants of NEIL2 were used for immunoblot analysis using ECL system, as per manufacturer's protocol (Amersham Pharmacia).

Analysis of trapped NEIL2 complexes

A ^{32}P -labeled duplex oligo (100 fmol) containing 5-OHU•G was incubated with lysates (1 μg) of *E. coli* expressing WT or mutant NEIL2 in 15 μl assay buffer in the presence of 25 mM NaCNBH_3 at 37°C for 30 min. The trapped complexes were then separated by SDS-PAGE (12% polyacrylamide), as described previously (10).

Purification of wild-type and mutant NEIL2

The recombinant WT NEIL2 polypeptide was purified as before (10). Two of the mutant proteins, namely, C291S and H295A were also purified similarly with some protocol modifications. Briefly, after Polymin P precipitation, the ammonium sulfate fractionated pellets were dialyzed in buffer A (25 mM Tris-HCl, pH 7.5, 10% glycerol, and 0.5 mM DTT) containing 100 mM NaCl and passed through 5 ml Q- and SP-Sepharose (Amersham Pharmacia) columns attached in tandem, which were then washed with 120 mM NaCl. The mutant NEIL2 proteins in the flowthrough was concentrated in an Amicon filter and loaded on to a 25-ml Superdex 75 column. The fractions eluted from Superdex were further purified by FPLC on Mono Q using NaCl gradient (20-200 mM) in buffer A. The NEIL2 mutants eluted at around 75

mM NaCl. The other two mutant proteins, C291S and C315S were subcloned into a C-terminal His tag-containing vector, pET22b (Novagen). After induction and sonication as before, the cells were spun down at 13 K and the supernatant loaded onto Ni-NTA (Ni²⁺-nitrilotriacetate)-agarose column (Qiagen), previously equilibrated with buffer B (40 mM Tris-HCl, pH 7.5, 1 M NaCl). After washing with buffer B, the His-tagged mutant proteins were eluted with an imidazole gradient (20 – 200 mM imidazole in Buffer B). After elution, the peak enzyme fractions were dialyzed against buffer C (25 mM Tris-HCl, pH 7.5, 50 mM NaCl, 1 mM DTT, 10 % glycerol). The enzymes were further purified by FPLC chromatography on MonoQ column like the untagged mutants. The arginine mutant R310Q was also His-tagged in the C-terminus, and purified from the extract of plasmid-bearing *E. coli* by affinity chromatography on Ni-NTA-agarose (Qiagen). After elution with 150 mM imidazole, the enzyme was dialyzed against 25 mM Tris-HCl, pH 7.5, 50 mM NaCl and finally purified on a MonoS column. Purified preparations of WT or mutant NEIL2 proteins were never frozen and were stored at -20°C in PBS containing 50% glycerol.

Incision assay with 5-OHU-containing bubble oligo

DNA strand cleavage at the abasic (AP) site after damaged base excision by NEIL2 occurs due to its intrinsic AP lyase activity. We have shown previously that NEIL2 has higher activity when the lesion is inside a bubble in an otherwise duplex oligo (14). The strand incision by NEIL2 was used for its assay using a oligo containing 5-OHU in the middle of unpaired 11 nt bubble (B11), as described previously (14). The 51-mer oligo, ³²P-labeled at the 5' terminus of the lesion-containing strand, was incubated with NEIL2 (WT and mutants) at 37°C for 15 min in a 15 µl reaction mixture containing 40 mM Hepes (pH 7.5), 50 mM KCl, 100 µg/ml bovine serum albumin and 5% glycerol. After the reaction was stopped with 80% formamide and 20

mM NaOH, the cleaved oligos were separated by denaturing gel electrophoresis in 15% polyacrylamide containing 7 M urea in 90 mM Tris-borate (pH 8.3), 2 mM EDTA. The radioactivity in the substrate and cleaved product was analyzed by PhosphorImager (Amersham Biosciences).

Electrophoretic gel mobility shift assay

The wild type and mutant NEIL2 (C291S, H295A, C315S, C318S, and R310Q) were incubated with a 5'-³²P-labeled 5-OHU-containing bubble oligo (5-OHU•B11) in 10 µl buffer containing 25 mM Hepes-KOH, pH 7.6, 50 mM NaCl, 0.5 mM EDTA, 0.5 mM DTT, 10 µg/ml poly dI-dC and 12% glycerol at 20°C for 15 min, followed by electrophoresis in 6% nondenaturing polyacrylamide gel containing 25 mM Tris-HCl, pH 7.5; 55 mM borate; and 0.6 mM EDTA (pH 7.4) at room temperature. The radioactivity in the shifted DNA protein complex was analyzed by PhosphorImager.

Quantitation of zinc in NEIL2

The zinc content of wild type and mutant NEIL2 polypeptides was determined by inductively coupled plasma mass spectrometry. The enzymes were dialyzed against PBS prior to analysis of Zn²⁺ using a calibration curve with known amounts of Zn²⁺. The Zn content of the enzymes was corrected for contamination in the dialysis buffer.

Circular dichroism spectroscopy

All CD spectra were collected from proteins after dialysis and filtration in an AVIV 60DS spectrometer at 25°C. An average of three scans of the spectra (250 to 200 nm) was used to obtain the final data. The molar ellipticity (θ) was calculated using the following equation:

$$\theta = \frac{\theta_{obs} \times 10^{-3} \times MW}{C \times l \times n \times 10^{-2}} \text{ deg } dmole^{-1} cm^2$$

where θ_{obs} is the observed ellipticity; MW, molecular weight; C, concentration (mg/ml); l, the pathlength of the cuvette in cm and n, the number of residues. Protein concentrations were determined by the Bradford Assay using bovine serum albumin as the standard.

Molecular modeling of 192-319 residues of NEIL2

The sequence of NEIL2 with the potential DNA binding region (residues 192-319) was used as the seed sequence to search for a suitable template using BIOSERVER (meta server located at <http://bioserv.cbs.cnrs.fr/>). BIOSERVER submits to fold-recognition servers like 3D-PSSM (28), mGenThreade (29) Sam-T99 (30) and PDB-BLAST. The results from different servers are parsed automatically and the TITO program is used to evaluate most compatible template (31). The crystal structure of *E. coli* formamidopyrimidine-DNA glycosylase (Fpg/MutM, PDB code: 1k82) (32) was selected as the most favorable template, with a TITO score of -68248 (PDB-BLAST score for this template: $1e^{-37}$, SAM-T99 score: $4.37e^{-42}$, 3DPSSM score: $2.7e^{-3}$, mGenThreader score for 1ee8 template: $3e^{-4}$). The initial alignment was improved to minimize gaps in the beta or helix regions, and the final alignment had an identity of 30% to the template. Distance and dihedral constraints were extracted from the template using the geometry extraction program EXDIS, available in the homology modeling package MPACK(33-35). Structurally conserved regions or the fragments defined by excluding gaps in the pair-wise alignment were used to extract geometric constraints. Upper and lower distance constraints were defined either by adding or subtracting a threshold of 0.25 Å to the actual distance for matching side-chain and main-chain (backbone) atoms. To position the side chains of C291, H295, C315, and C318, additional distance constraints among heavy side chain atoms were extracted from a CHCC type zinc finger found in the DNA-binding domain of RAG1 (PDB code:1rmd,

residues:C41, H43,C61,C64). Upper- and lower-bound dihedral angle constraints were defined by adding or subtracting 5°. A total of 30 distance constraints per atom were extracted from the matching regions of the template. Models were generated using the distance geometry program DIAMOD. A few cycles of constrained energy minimization were applied using the program FANTOM which minimizes constraint energies by successive application of quasi-Newton and Newton-Raphson minimizers (36), using the ECEPP/2 force field. The conformational energy of the model after energy minimization was - 410 kcal/mol.

Results

Expression and activity of WT and mutant NEIL2 in crude E. coli extracts

Sequence alignment of NEIL2 with Fpg and Nei predicted that NEIL2 is a Zn-finger protein with a CHCC-type motif near the C-terminus. C291, H295, C315 and C318 are candidate residues for coordinating Zn²⁺ (Fig 1). This motif is distinct from the Zn-finger motifs of Nei/Fpg, which are of the CCCC type (17). Single point mutants of NEIL2, C291S, H295A, C315S and C318S were expressed in *E. coli*, and their expression was monitored by Western analysis (Fig 2A). The mutations did not affect expression of NEIL2 in *E. coli*, as indicated by the presence of a protein band of the predicted size in each induced bacterial lysate. In *E. coli* expressing the H295A mutant, a protein with slight slower migration was observed which was not present (lane 2) in the control extract of *E. coli*, expressing the empty vector. This band should thus be the H295A mutant of NEIL2. This analysis also underscored the strong specificity of the antibody.

All DNA glycosylases/AP lyases, regardless of their substrate preference, form transient Schiff bases with free AP site in DNA, which could be reduced with NaCNBH₃ (or NaBH₄) to form a stable “trapped complex” (37,38). We have shown earlier that NEIL2, like other

MutM/Nei type enzymes, is inactivated when the N-terminal Pro, the active site nucleophile, is blocked or eliminated (10). Fig.2B shows SDS-PAGE separation of ³²P-labeled trapped complexes generated with extracts of *mutM nei E. coli* harboring WT or mutant NEIL2 expression plasmids after incubation of 5-OHU•G-containing oligo. Because the mobility of such complexes reflects the size of the DNA glycosylase when the same oligo substrate is used, it is evident that in control *E. coli* lacking Fpg and Nei, only endogenous Nth formed a major trapped complex (lane 3). Crude bacterial lysates harboring WT NEIL2 formed a trapped complex of the same size as the purified recombinant NEIL2 (lane 2) used as a marker. However, the lack of such trapped complexes with crude lysates expressing various mutant NEIL2 proteins (lanes 5-8) suggests that the mutants are inactive as AP lyases. This loss of activity is likely to be due to loss of the Zn-finger motif, critical either for structural integrity or the DNA-binding activity of this enzyme.

DNA-binding and incision activity of purified WT and mutant NEIL2

Wild type and NEIL2 mutants (C291S, C315S, C318S, H295A, and R310Q) were purified to apparent homogeneity (Fig 3). Surprisingly, the H295A mutant migrated abnormally and ran more slowly than the WT or the other mutants. We have shown earlier that NEIL2 is active in excising several cytosine-derived lesions and has robust activity for 5-OHU in bubble DNA (14). Purified WT and mutant NEIL2 polypeptides were tested for DNA incision assays with a 5-OHU-containing bubble oligo (5 OHU• B11). The expected $\beta\delta$ -elimination product, i.e., cleaved 5-OHU containing strand with 3' phosphate termini, was observed with the WT NEIL2 protein (14). However, neither mutant NEIL2 generated the oligo fragment to a detectable extent (Fig. 4A). The WT and mutant proteins were also assayed for their DNA-binding activity by gel mobility shift assay with 5 OHU -containing 11-nt bubble (B11) oligo.

Again the DNA protein complex was observed only with WT NEIL2 (lane 2) but not the mutant proteins (lanes 3-6; Fig. 4B).

Zinc content of wild type and mutant NEIL2

Purified WT and C318S and H295A mutant NEIL2 were analyzed for zinc content by ICP-MS. The WT NEIL2 protein contained 0.97 ± 0.086 mol zinc/mol of protein. In contrast, C318S and H295A mutants contained less than 0.1 mol of zinc/mol protein (Table 1).

Structural alterations in H295A and C318S NEIL2 mutants

The presence of zinc was shown to be essential for the folding and stability of many classical Zn^{2+} -finger proteins. Based on our results that C291, H295, C315 and C318 residues are responsible for coordinating Zn^{2+} , we examined the effect of mutation in these residues on the secondary structure of the protein by analyzing the circular dichroism (CD) spectra of purified WT and two mutant NEIL2 (H295A and C318S) proteins. The far-UV CD spectrum (Fig 5) shows that WT NEIL2 has distinct secondary structure, as indicated by the minima in molar ellipticity at 208 and 222 nm. However, the CD spectra of both the H295A and C318S proteins showed strong reduction in the mean residue ellipticity. These results indicate gross structural changes induced by mutations at His 295 or Cys 318 of NEIL2.

Molecular model of NEIL2 residues 192-319

A homology model of C-terminal residues (192-319) of NEIL2 was built using *E. coli* Fpg (PDB code: 1k82) (32). The structural alignment used for the modeling is represented in Fig. 6A. The final model (Fig. 6B) showed backbone RMSD value of 0.55 Å to the template. The model consists of four helices formed by residues 203-208, 216-220, 231-241, 254-271, a 3_{10} -helix by residues 249-251, and a beta sheet formed consisting of two beta strands formed by residues 300-302 and 312-314. The model has helix-two turn-helix motif formed by four helices

and a novel beta-hairpin CHCC type zinc finger. The CHCC type zinc finger is formed by residues C291, H295, C315 and C318. Mutations in any one of these residues abolish the function of NEIL2. The beta hairpin zinc finger provides a necessary structural framework to position the conserved R310 that may take part in the catalytic reaction. By superimposing the model on the co-crystal structure of DNA bound to *E. coli* Fpg (PDB code: 1k82), we found that the conserved R310 (Fig. 6C) is placed in a position similar to R258 in *E. coli* Fpg (32). Thus our model of human NEIL2 provides a mechanistic insight into the tertiary structure of the protein. The model is available at <http://www.rcsb.org> (PDB code: 1vzp).

Requirement of Arg310 for enzyme activity

To clarify the role of the conserved Arg residue identified by molecular modeling (Fig.6C), we constructed and characterized the NEIL2 site-directed mutant, R310Q. The purified R310Q protein showed greatly diminished activity relative to the WT NEIL2 with a 5OHU containing bubble DNA substrate (Fig. 7A), and also decreased DNA binding (Fig. 7B). These results thus further confirm that the zinc finger positions the conserved Arg 310 correctly in the active site pocket of NEIL2.

Discussion

Zinc is an essential trace element, and the second most abundant metal in mammalian cells. The adult human body contains ~3g of Zn²⁺ (39). It plays key roles in the maintenance of chromatin structure, and also in nucleic acid metabolism as a structural component of enzymes in DNA replication, transcription and DNA repair (40). The binding of zinc stabilizes the folded conformations of protein domains so that they may facilitate interactions with other macromolecules such as DNA. The lack of redox activity for the zinc ion and its binding and exchange kinetics may also be important in the use of zinc for specific functional roles, unlike

other transition metal ions which might engage in free radical generation, leading to carcinogenic oxidative damage in cells (41). The peptide motifs containing bound Zn and named “zinc fingers” in proteins were first identified about 20 years ago during investigation of eukaryotic transcription factors. Since then more than 10 different classes of Zn-finger motifs have been discovered and characterized, many for their ability to bind nucleic acids in a sequence-specific manner, and others for specifically mediating protein-protein interactions (42). Unlike the typical mode of Zn^{2+} coordination within the catalytic center of enzymes, tetrahedral coordination of Zn^{2+} in zinc fingers characteristically involves two to four potentially redox-reactive sulfhydryl groups (cysteine). It is estimated that zinc finger proteins constitute up to 1% of all human gene products, with each of these proteins containing from 1 to 30 repeats of cysteine (+ histidine) - containing zinc finger motifs.

NEIL1 and NEIL2 are two orthologs of *E. coli* Fpg/Nei, which were shown to be Zn finger proteins. Although NEIL1 and NEIL2 have significant functional overlap and use the same reaction chemistry as Fpg and Nei, only NEIL2 possesses a potential Zn-finger motif. Near the C-terminus, it contains a unique sequence with three Cys and one His residues in an unusual Zn-finger configuration (Fig. 1), that is not homologous to the Zn finger motifs of Nei/Fpg. In this study we set out to confirm that NEIL2 is indeed a Zn-finger protein, and then to examine the role of this motif in the structure and function of this glycosylase.

We used site-directed mutagenesis to confirm the requirement for the 3 Cys and 1 His residues predicted to coordinate with Zn in the putative zinc finger domain of NEIL2. The DNA-trapping assay is a fast and definitive method for assessing the base excision activity of DNA glycosylase/AP lyases. Because trapped complexes with a radiolabeled oligo can be separated by SDS-PAGE that can identify glycosylases based on their mobility (43), we tested whether any of

the mutant proteins has DNA glycosylase/AP lyase activity. The absence of trapped complexes with all four mutants confirmed that mutation of any one of these Cys and His residues totally abolished the enzymatic activity (Fig. 2). This is consistent with a critical role for the Zn finger in enzymatic function, as was also observed for Fpg and Nei (44,45). We then tested whether the loss of enzymatic activity was due to loss of DNA-binding activity. We carried out EMSA with purified WT and mutant proteins using a 5 OHU-containing bubble substrate oligo. All the cysteine mutants and the single histidine mutant failed to bind substrate DNA, indicating that the Zn-finger motif is essential for DNA binding. Subsequent studies confirmed that the purified mutant NEIL2s have no strand incision activity with the substrate oligo (Fig. 4). Finally, mass spectroscopic analysis showed that the WT NEIL2 contained 1 mol of Zn per mol of protein while the mutants (C318S and H295A) lacked bound Zn²⁺ (Table1). This provided the strongest evidence that the candidate Cys and His residues are indeed responsible for Zn coordination, and that the mutation of even one residue abolishes this coordination. This raised the question as to whether the loss of Zn²⁺ induces any change in the secondary structure of NEIL2. The CD spectrum clearly showed that the secondary structures of the C318S and H295A mutants were drastically altered (Fig. 5). Mutations in these residues are likely to prevent proper folding of the beta strands into a hairpin motif (Fig. 6B) and hence the geometry of the critical conserved residue R310 (predicted from the model) may not be situated correctly. Mutation of R310 strongly reduced NEIL2 activity without significantly affecting DNA binding (Fig. 7), unlike the mutations in Zn co-ordinating residues. This strongly suggests that R310 in NEIL2, positioned by the zinc-binding pocket is highly conserved as in the Fpg/Nei family and performs an indispensable catalytic role similar to that of R258 in *E. coli* Fpg (32), or R253 in *E. coli* Nei (46). In both case, this residue participates in protonation of 5'-phosphate. It was recently shown

that the conserved Arg is also present in the other mammalian *nei* homolog, NEIL1 (47).

Although mammalian NEIL1 has similar folds as the bacterial Fpg/Nei, it has an unusual motif near the C-terminus. This structural motif mimics the β -hairpin zinc finger found in members of the Fpg/Nei class, (including NEIL2) but lacks the loops harboring the canonical zinc-binding residues, and therefore does not co-ordinate zinc. Interestingly, the critical Arg, R277 in NEIL1, is positioned in the loop connecting the two β -strands of the zincless finger, and its mutation to Ala showed a strong reduction of glycosylase activity (47). We have shown here that the R310Q mutant of NEIL2 also has markedly reduced glycosylase activity. Thus the conserved Arg is positioned critically for glycosylase activity in both the zinc-containing (NEIL2 and Fpg/Nei) and zinc-less fingers (NEIL1).

Our studies thus reveal that the localized destabilization of the Zn-finger motif in NEIL2 affected the conformation of the whole polypeptide. The structural perturbation in the mutants was also reflected during purification. The WT NEIL2 binds strongly to the SP resin during FPLC. In contrast, the zinc finger mutants did not bind to SP, and bound weakly to the Q column. Taken together, our results provide definitive evidence for the identity of Zn-coordinating residues and show that the zinc-finger motif is integral to the structure and function of NEIL2. We may note in passing that the nonconsensus (CHCC type) motif is rather uncommon among the Zn finger proteins involved in DNA metabolism.

Further work with high resolution X-ray diffraction analysis will provide a more detailed understanding about specific residues involved in maintenance of the Zn finger domain and overall stability of the protein. A larger implication of this study involves public health issues such as malnutrition and hence lower Zn levels in the diet (48) or exposure to chemical toxins or

radiation, which induce oxidative stress, could inactivate NEIL2, leading to reduced repair of oxidative damage of the genome.

Acknowledgements

We thank Dr. Robert Surfass, UTMB, Galveston for measuring zinc by ICP-MS and Lucy Lee for CD spectroscopic analysis. We thank Werner Braun, Sealy Center for Structural Biology, UTMB for MPACK program and valuable suggestions. We acknowledge Dr. David Konkel for critically reviewing the manuscript and Wanda Smith for expert secretarial assistance. This work was supported by USPHS grants, RO1 CA81063 and PO1 CA92584.

Abbreviations

The following abbreviations were used: AP, abasic; BER, base excision repair; DTT, dithiothreitol; Fpg, FapyG-DNA glycosylase; ICP-MS, inductively coupled plasma mass spectrometry; Nei, endonuclease VIII; NTH, endonuclease III homolog; NEIL, Nei-like; OGG, 8-oxoguanine-DNA glycosylase; PBS, phosphate buffered saline; WT, wild type; RMSD, root mean square deviation.

References

1. Ames, B. N., Shigenaga, M. K., and Hagen, T. M. (1993) *Proc Natl Acad Sci U S A* **90**, 7915-7922
2. Breen, A. P., and Murphy, J. A. (1995) *Free Radic Biol Med* **18**, 1033-1077
3. Krokan, H. E., Standal, R., and Slupphaug, G. (1997) *Biochem J* **325** (Pt 1), 1-16
4. Ikeda, S., Biswas, T., Roy, R., Izumi, T., Boldogh, I., Kurosky, A., Sarker, A. H., Seki, S., and Mitra, S. (1998) *J Biol Chem* **273**, 21585-21593
5. Lu, R., Nash, H. M., and Verdine, G. L. (1997) *Curr Biol* **7**, 397-407
6. Boiteux, S. (1993) *J Photochem Photobiol B* **19**, 87-96
7. Jiang, D., Hatahet, Z., Blaisdell, J. O., Melamed, R. J., and Wallace, S. S. (1997) *J Bacteriol* **179**, 3773-3782
8. Zharkov, D. O., Rieger, R. A., Iden, C. R., and Grollman, A. P. (1997) *J Biol Chem* **272**, 5335-5341
9. Hazra, T. K., Izumi, T., Boldogh, I., Imhoff, B., Kow, Y. W., Jaruga, P., Dizdaroglu, M., and Mitra, S. (2002) *Proc Natl Acad Sci U S A* **99**, 3523-3528
10. Hazra, T. K., Kow, Y. W., Hatahet, Z., Imhoff, B., Boldogh, I., Mokkalpati, S. K., Mitra, S., and Izumi, T. (2002) *J Biol Chem* **277**, 30417-30420
11. Bandaru, V., Sunkara, S., Wallace, S. S., and Bond, J. P. (2002) *DNA Repair (Amst)* **1**, 517-529
12. Rosenquist, T. A., Zaika, E., Fernandes, A. S., Zharkov, D. O., Miller, H., and Grollman, A. P. (2003) *DNA Repair (Amst)* **2**, 581-591
13. Takao, M., Kanno, S., Kobayashi, K., Zhang, Q. M., Yonei, S., van der Horst, G. T., and Yasui, A. (2002) *J Biol Chem* **277**, 42205-42213

14. Dou, H., Mitra, S., and Hazra, T. K. (2003) *J Biol Chem* **278**, 49679-49684
15. Thayer, M. M., Ahern, H., Xing, D., Cunningham, R. P., and Tainer, J. A. (1995) *Embo J* **14**, 4108-4120
16. Sugahara, M., Mikawa, T., Kumasaka, T., Yamamoto, M., Kato, R., Fukuyama, K., Inoue, Y., and Kuramitsu, S. (2000) *Embo J* **19**, 3857-3869
17. Zharkov, D. O., Shoham, G., and Grollman, A. P. (2003) *DNA Repair (Amst)* **2**, 839-862
18. Brown, R. S., Sander, C., and Argos, P. (1985) *FEBS Lett* **186**, 271-274
19. Miller, J., McLachlan, A. D., and Klug, A. (1985) *Embo J* **4**, 1609-1614
20. Kadonaga, J. T., Carner, K. R., Masiarz, F. R., and Tjian, R. (1987) *Cell* **51**, 1079-1090
21. Falchuk, K. H. (1993) *Prog Clin Biol Res* **380**, 91-111
22. Tanaka, K., Miura, N., Satokata, I., Miyamoto, I., Yoshida, M. C., Satoh, Y., Kondo, S., Yasui, A., Okayama, H., and Okada, Y. (1990) *Nature* **348**, 73-76
23. Menissier-de Murcia, J., Molinete, M., Gradwohl, G., Simonin, F., and de Murcia, G. (1989) *J Mol Biol* **210**, 229-233
24. Mazen, A., Menissier-de Murcia, J., Molinete, M., Simonin, F., Gradwohl, G., Poirier, G., and de Murcia, G. (1989) *Nucleic Acids Res* **17**, 4689-4698
25. Bochkareva, E., Korolev, S., and Bochkarev, A. (2000) *J Biol Chem* **275**, 27332-27338
26. Navaratnam, S., Myles, G. M., Strange, R. W., and Sancar, A. (1989) *J Biol Chem* **264**, 16067-16071
27. Doolittle, R. F., Johnson, M. S., Husain, I., Van Houten, B., Thomas, D. C., and Sancar, A. (1986) *Nature* **323**, 451-453
28. Bates, P. A., Kelley, L. A., MacCallum, R. M., and Sternberg, M. J. (2001) *Proteins Suppl* **5**, 39-46

29. McGuffin, L. J., Bryson, K., and Jones, D. T. (2000) *Bioinformatics* **16**, 404-405
30. Karplus, K., Barrett, C., and Hughey, R. (1998) *Bioinformatics* **14**, 846-856
31. Labesse, G., and Mornon, J. (1998) *Bioinformatics* **14**, 206-211
32. Gilboa, R., Zharkov, D. O., Golan, G., Fernandes, A. S., Gerchman, S. E., Matz, E., Kycia, J. H., Grollman, A. P., and Shoham, G. (2002) *J Biol Chem* **277**, 19811-19816
33. Mathura, V. S., Soman, K. V., Varma, T. K., and Braun, W. (2003) *J Mol Model (Online)* **9**, 298-303
34. Ivanciuc, O., Oezguen, N., Mathura, V. S., Schein, C. H., Xu, Y., and Braun, W. (2004) *Curr Med Chem* **11**, 583-593
35. Hasan, R. J., Pawelczyk, E., Urvil, P. T., Venkatarajan, M. S., Goluszko, P., Kur, J., Selvarangan, R., Nowicki, S., Braun, W. A., and Nowicki, B. J. (2002) *Infect Immun* **70**, 4485-4493
36. Schaumann, T., Braun, W., and Wuthrich, K. (1990) *Biopolymers* **29**, 679-694
37. McCullough, A. K., Dodson, M. L., and Lloyd, R. S. (1999) *Annu Rev Biochem* **68**, 255-285
38. Hill, J. W., Hazra, T. K., Izumi, T., and Mitra, S. (2001) *Nucleic Acids Res* **29**, 430-438
39. Berg, J. M., and Shi, Y. (1996) *Science* **271**, 1081-1085
40. Laity, J. H., Lee, B. M., and Wright, P. E. (2001) *Curr Opin Struct Biol* **11**, 39-46
41. Baldwin, M. A., and Benz, C. C. (2002) *Methods Enzymol* **353**, 54-69
42. Krishna, S. S., Majumdar, I., and Grishin, N. V. (2003) *Nucleic Acids Res* **31**, 532-550
43. Hazra, T. K., Izumi, T., Maitt, L., Floyd, R. A., and Mitra, S. (1998) *Nucleic Acids Res* **26**, 5116-5122

44. O'Connor, T. R., Graves, R. J., de Murcia, G., Castaing, B., and Laval, J. (1993) *J Biol Chem* **268**, 9063-9070
45. Tchou, J., Michaels, M. L., Miller, J. H., and Grollman, A. P. (1993) *J Biol Chem* **268**, 26738-26744
46. Zharkov, D. O., Golan, G., Gilboa, R., Fernandes, A. S., Gerchman, S. E., Kycia, J. H., Rieger, R. A., Grollman, A. P., and Shoham, G. (2002) *Embo J* **21**, 789-800
47. Doublet, S., Bandaru, V., Bond, J. P., and Wallace, S. S. (2004) *Proc Natl Acad Sci U S A* **101**, 10284-10289
48. Ho, E., Courtemanche, C., and Ames, B. N. (2003) *J Nutr* **133**, 2543-2548
49. Koradi, R., Billeter, M., and Wuthrich, K. (1996) *J Mol Graph* **14**, 51-55, 29-32

Figure Legends

Figure 1: *Putative Zn finger domain of NEIL2.* **A.** Amino acid sequence alignment of NEIL2 with *E. coli* Nei and Fpg. The C-termini of Nei and Fpg were aligned with the C-terminal sequence of NEIL2. The position of the helix two turn helix motif (H2TH) is indicated and the coordinating amino acid residues forming the zinc finger motif were boxed. **B.** Schematic diagram of the C terminus of NEIL2 bearing the putative zinc finger motif.

Figure 2: *Expression and activity of WT and mutant NEIL2 in crude E. coli extracts.* **A.** Western analysis of soluble extract of *E. coli* expressing wild-type and mutant NEIL2. An arrow indicates the position of migration of the purified recombinant NEIL2 protein (Lane1). **B.** Analysis of trapped complexes with extracts of *E. coli* expressing WT and mutant NEIL2. 5'-³²P-labelled 5-OHU•G (0.1 pmol) was incubated with no protein, recombinant NEIL2, vector control and *E. coli* extracts in the presence of NaCNBH₃ before SDS/PAGE. The positions of free DNA and trapped complexes of purified NEIL2 and *E. coli* Nth (as marker) are indicated. Other details are given in Experimental Procedures.

Figure 3: *Purification of WT and mutant NEIL2.* WT (lane 1), C291S, H295A, R310Q, C315S, and C318S mutant NEIL2 (lanes 3-7) proteins purified as described in Experimental Procedures were analyzed by 12% SDS-PAGE. Lane 2, size markers (BioRad).

Figure 4: *DNA incision and binding activities of purified WT and mutant NEIL2.* **A.** DNA incision assay. C291S, H295A, C315S and C318S mutants (50 nM, lanes 3 - 6) and WT NEIL2 (lane 2), were incubated with 5' ³²P-labeled 5-OHU-

containing 11 nt bubble oligo (250 nM) and the reaction products were separated by denaturing gel electrophoresis. S, indicates substrate and P, the position of products in the gel. **B.** DNA binding assay. 5' ³²P-labeled 5-OHU-containing 11-mer bubble (0.2 pmol) was incubated with 5 ng each of purified WT (lane 2), C291S (lane 3), H295A (lane 4), C315S (lane 5) and C318S (lane 6) for gel mobility shift analysis in 6% polyacrylamide.

Figure 5: *CD spectra of purified WT and mutant NEIL2.* Far-UV CD spectra of WT and mutant NEIL2 (H295A and C318S) in PBS (pH 7.0) at 25°C.

Figure 6: *Model of residues 192-319 of NEIL2.* **A.** Structural alignment for NEIL2 and *E. coli* Fpg (1K82) template generated by 3DPSSM. Identical residues are indicated by '*'. Residues that participate in co-ordination of zinc ion are highlighted in red and bold face. **B.** Ribbon diagram of a model of C-terminal region of NEIL 2 generated using MOLMOL (49). The helices (shown in green) form the helix two turn helix motif that binds to DNA. CHCC type beta hairpin zinc finger is highlighted with coordinating residues Cys 291, His 295, Cys 315 and Cys 318. **C.** Ribbon diagram of model of C-terminal region of NEIL 2 with DNA, generated with MOLMOL. The helices (shown in blue) form the helix two turn helix motif that binds to DNA. CHCC type beta hairpin zinc finger is highlighted with coordinating residues Cys 291, His 295, Cys 315, Cys 318. The Zinc ion stabilizes beta strands (shown in green) that is critical to position the catalytic residue Arg 310 which is conserved in *E. coli* Fpg.

Figure 7: *Incision and binding activities of R310Q mutant.* **A.** Comparative DNA glycosylase/ AP lyase activities of WT (lanes 2 – 5; 2.5, 5, 10, 20 ng protein

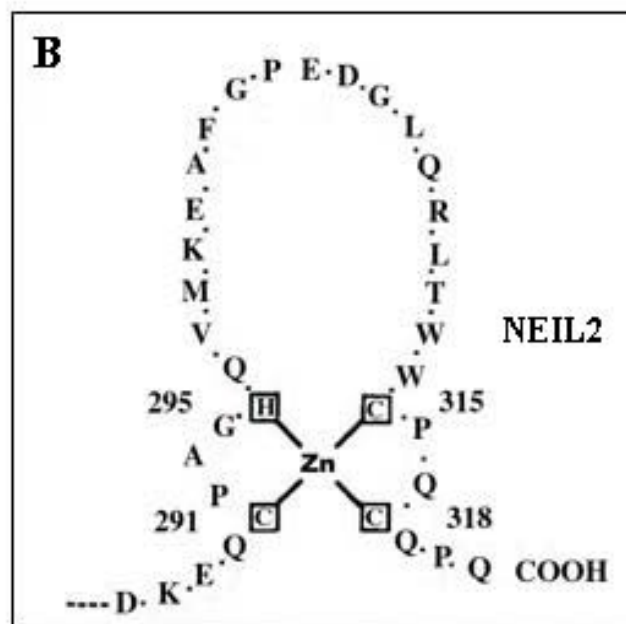
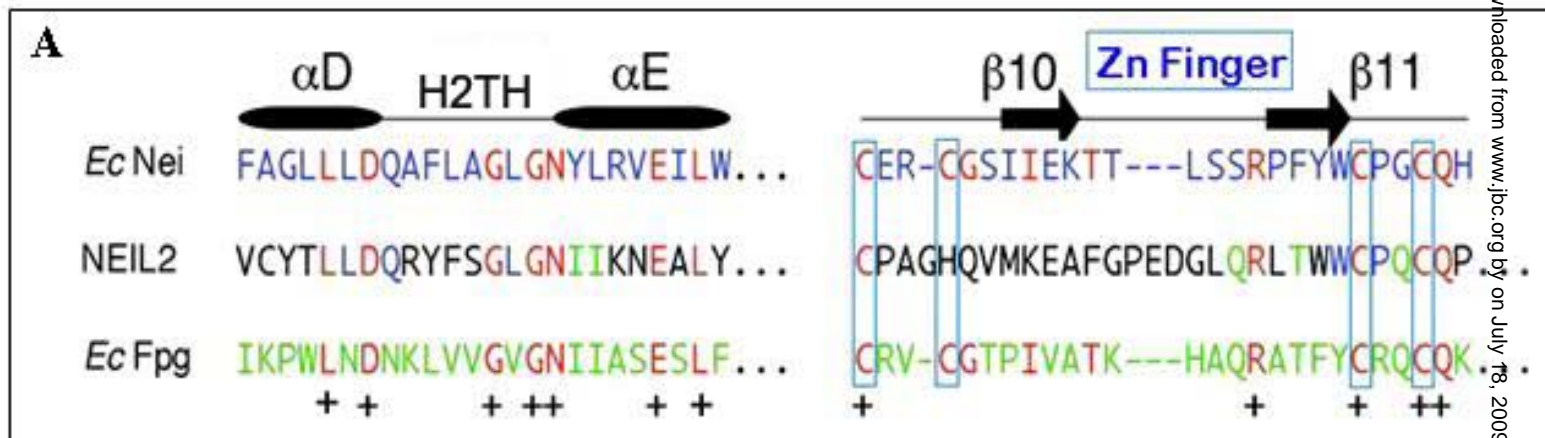
respectively) and R310Q (lanes 6–9, 2.5, 5, 10, 20 ng protein respectively) NEIL2 on 5-OHU•B11 (2.5 pmol). Lane 1, no enzyme. S, substrate; P, product. **B.**

DNA- binding analysis of WT (lane 2) and R310Q (lane 3) with 5-OHU•B11.

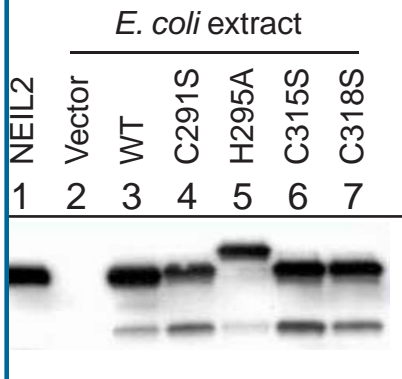
Lane1, No protein.

Table 1. Analysis of Zn content in WT and mutant NEIL2 by ICP-MS

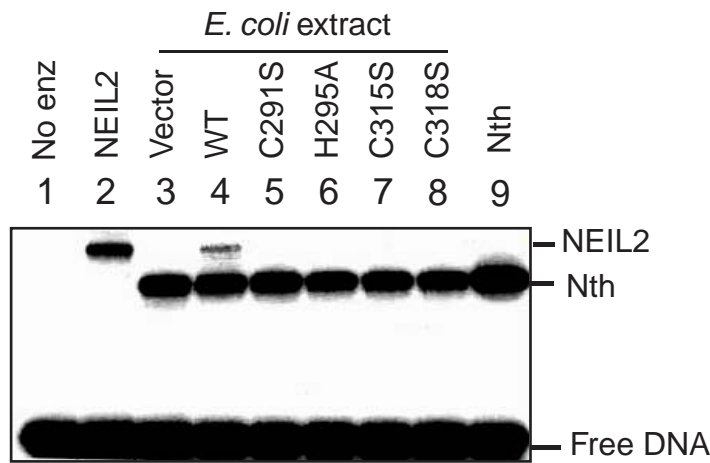
NEIL2 Proteins	Mol. of Zinc/Mol. of NEIL2
Wild Type	0.97 ± 0.086
C318S	0.15 ± 0.014
H295A	0.08 ± 0.009



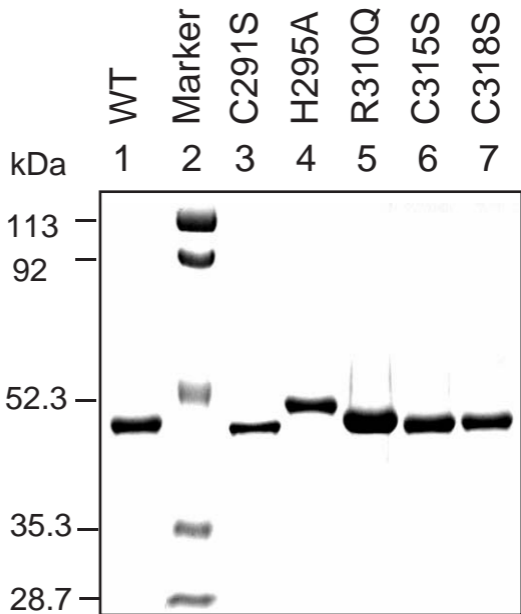
Western blot



B. Trapping assay

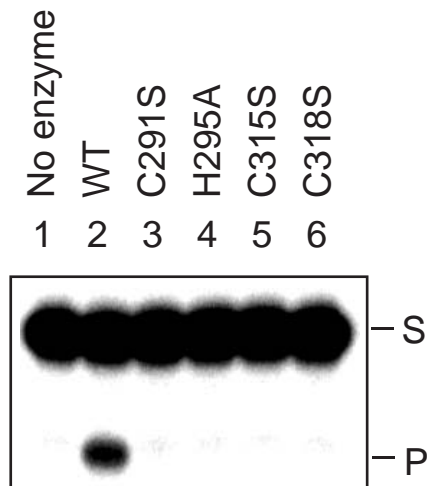


3. Das et al

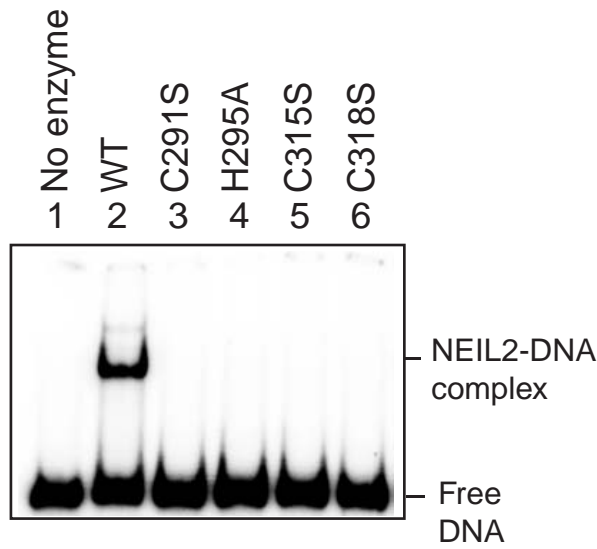


4. Das et al

A. Incision assay



B. Gel shift



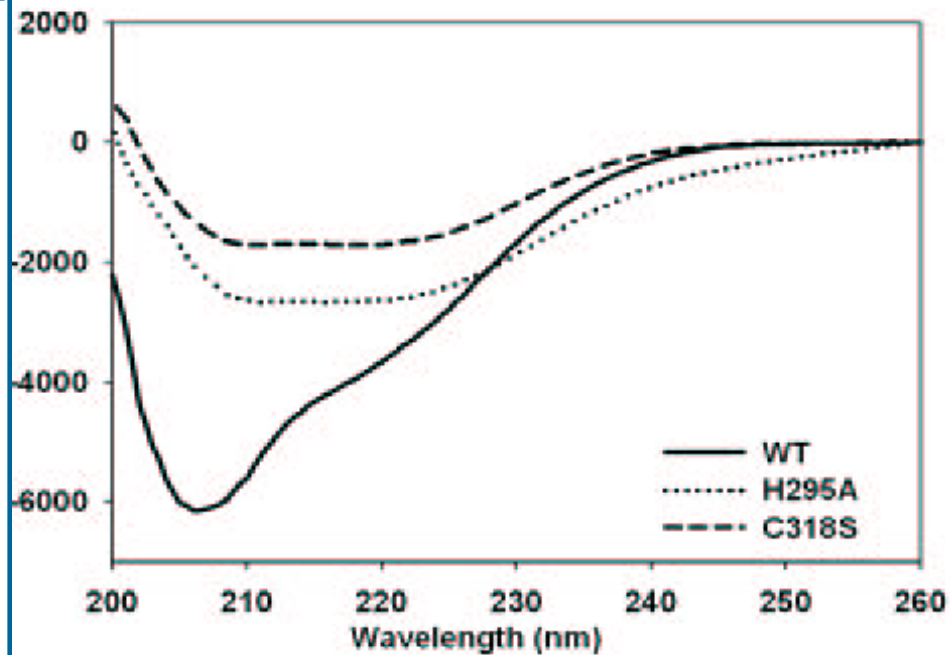
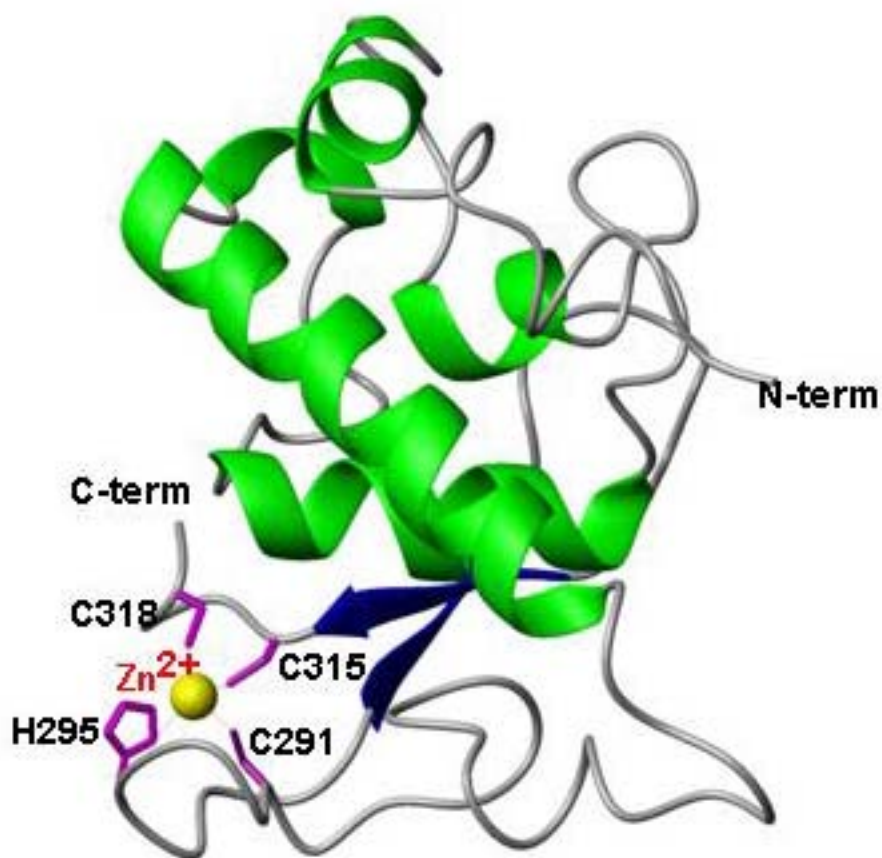


Fig 6. Das et al

A

NEIL2	PTCDILSEKFHRGQALEAL-GQAQPVCTLLDQRYFSGLGNI IKNEALYRAGIHPLSLGS
1K82	--PEPLSDDFNGEYLHQKCAKKKTAIKPWLMDNKLWVGVGNIYASESLFAAGIHPDRLAS
	** * * * * *** * * ***** * *
NEIL2	VL SASRREVLVDHVVEFSTAWLQG-----KFQGRPQHTQVYQK--EQCPAGHQVMKEAFG
1K82	SLSLAECCELLARVIKAVL LRSIEQGGTTLKPGYFAQELQVYGRKGEPCRV-CGTPIVATK
	** * * * * *** * * *
NEIL2	PEDGLQRLTWWCPCQC-
1K82	H---AQRATFYCRQCQK
	** * ***

B



C

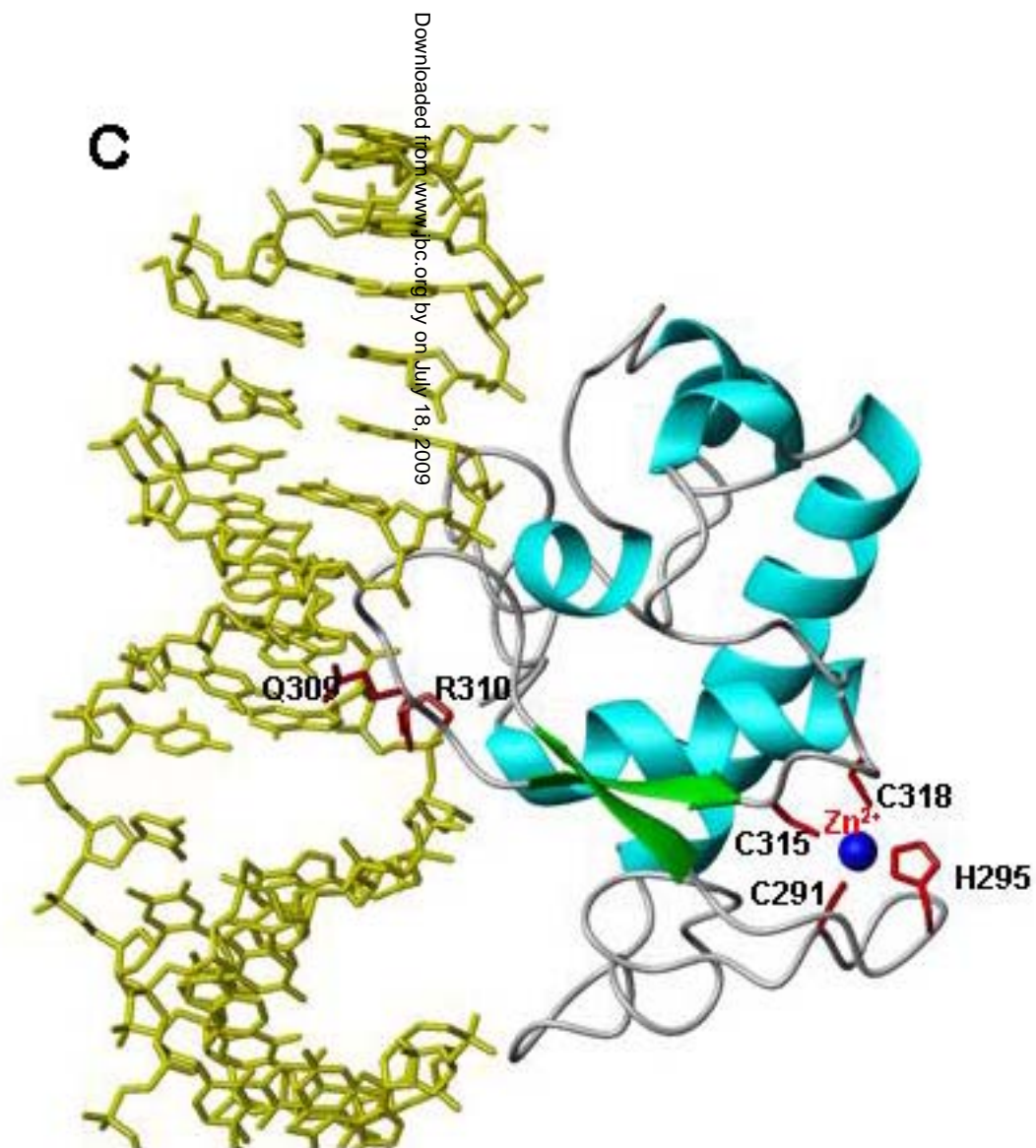
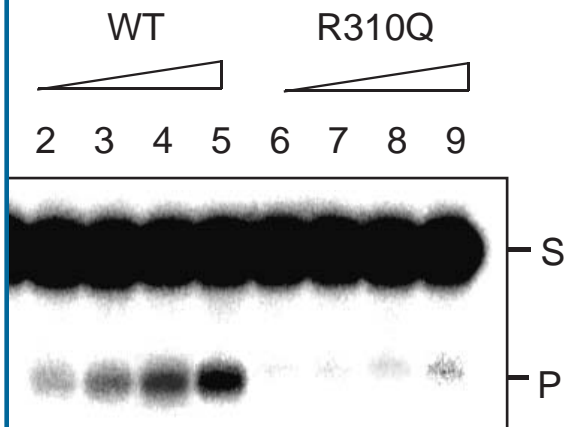


Fig 7. Das et al

ncision assay



B. Gel shift

